Front. Med. 2025, 19(1): 121−133
https://doi.org/10.1007/s11684-024-1103-5

RESEARCH ARTICLE

TRIM4 modulates the ubiquitin-mediated degradation of hnRNPDL and weakens sensitivity to CDK4/6 inhibitor in ovarian cancer

Xiaoxia Che*, Xin Guan*, Yiyin Ruan*, Lifei Shen, Yuhong Shen, Hua Liu, Chongying Zhu, Tianyu Zhou, Yiwei Wang (✉), Weiwei Feng (✉)

Department of Gynecology and Obstetrics, Ruijin Hospital Affiliated to Shanghai Jiao Tong University School of Medicine, Shanghai 200025, China

Abstract Ovarian cancer is the most lethal malignancy affecting the female reproductive system. Pharmacological inhibitors targeting CDK4/6 have demonstrated promising efficacy across various cancer types. However, their clinical benefits in ovarian cancer patients fall short of expectations, with only a subset of patients experiencing these advantageous effects. This study aims to provide further clinical and biological evidence for antineoplastic effects of a CDK4/6 inhibitor (TQB4616) in ovarian cancer and explore underlying mechanisms involved. Patient-derived ovarian cancer organoid models were established to evaluate the effectiveness of TQB3616. Potential key genes related to TQB3616 sensitivity were identified through RNA-seq analysis, and TRIM4 was selected as a candidate gene for further investigation. Subsequently, co-immunoprecipitation and GST pull-down assays confirmed that TRIM4 binds to hnRNPDL and promotes its ubiquitination through RING and B-box domains. RIP assay demonstrated that hnRNPDL binded to CDKN2C isoform 2 and suppressed its expression by alternative splicing. Finally, *in vivo* studies confirmed that the addition of siTRIM4 significantly improved the effectiveness of TQB3616. Overall, our findings suggest that TRIM4 modulates ubiquitin-mediated degradation of hnRNPDL and weakens sensitivity to CDK4/6 inhibitors in ovarian cancer treatment. TRIM4 may serve as a valuable biomarker for predicting sensitivity to CDK4/6 inhibitors in ovarian cancer.

Keywords TRIM4; CDK4/6 inhibitor; hnRNPDL; ovarian cancer

Introduction

Ovarian cancer (OC) has the worst prognosis and highest mortality rate among gynecological cancers [1]. Currently, cytoreductive surgery and platinum-based chemotherapy remain the most commonly used first-line treatments for OC [2]. Despite significant improvements in the diagnosis and treatment of OC, patients are typically diagnosed at an advanced stage, resulting in a 5-year survival rate of only 30% [3]. The recent introduction of poly(ADP-ribose) polymerase (PARP) inhibitors and antiangiogenic drugs has sparked notable progress in clinical oncology, with observed drug response rates ranging from 15% to 45% [2]. Therefore, there is an urgent need for novel and effective therapeutic strategies for OC.

Cyclin-dependent kinase-4 and kinase-6 (CDK4/6) are pivotal cell cycle kinases that regulate the G1–S transition by modulating the activation of the retinoblastoma protein (Rb). The hyperactivation of CDK4/6 is indispensable for the development and progression of numerous malignancies [4]. The discovery of CDK4/6 and their roles in cancer have led to the development of CDK4/6 inhibitors (CDK4/6is). Clinical trials have shown clear benefits in adding palbociclib, a small-molecule CDK4/6 inhibitor, to hormone antagonist therapy for breast cancer treatment, leading to its FDA approval in early 2015 [5,6]. CDK4/6is are also being tested as single agents or in combination with other targeted therapies in clinical trials for OC. A previous study found that Rb-deficient cell lines with low CCNE1 expression are sensitive to palbociclib [7]. However, the effectiveness of CDK4/6i in treating OC has not yet been determined, and biomarkers

Received March 26, 2024; accepted July 26, 2024
Correspondence: Yiwei Wang, wyw8Y743@rjh.com.cn;
Weiwei Feng, fww12066@rjh.com.cn

*These authors contributed equally.

indicating treatment effectiveness remain unidentified. The intrinsic negative regulation of CDK4/6 activity primarily occurs through mediation by the INK4 family of cell cycle inhibitors (INK4A, encoded by CDKN2A; INK4B, encoded by CDKN2B; INK4C, encoded by CDKN2C; and INK4D, encoded by CDKN2D), which bind to monomeric forms of CDK4/6 to form an inactive binary complex [4]. The inhibition of CDK4/6 has been demonstrated to impede the interaction of CDK4 and CDK6 with CDC37, a subunit of HSP90 that targets kinases, RB1 and other regulated genes [8].

Ubiquitination is a prevalent posttranslational modification that regulates a wide range of cellular processes. The initiation of ubiquitination involves the enzymes E1, E2, and E3 ubiquitin (Ub) activating, conjugating, and ligase enzymes, respectively. These enzymes facilitate the transfer of polyubiquitin to the target protein substrate, thereby triggering endocytosis signaling [9]. Various E3 ligases have been identified for their significant involvement in pathways associated with cancer hallmarks, functioning as both promoters and suppressors of tumorigenesis. These pathways encompass cell cycle progression, immune evasion, and tumor-promoting inflammation [10]. In the context of ovarian cancer, the oncogene MDM2 exhibits robust E3 ubiquitin-protein ligase activity and plays a crucial role in regulating p53 protein ubiquitination [11]. Additionally, the E3 ligase APC/C primarily mediates protein degradation associated with mitotic exit and acts as a suppressor of ovarian tumor progression [12,13].

TRIM4 is a member of the TRIM family, which belongs to the highly abundant E3 superfamily RING family. Like other TRIM proteins, TRIM4 contains four distinct motifs: the N-terminal RING domain, followed by the B-box domain, the coiled-coil (CC) core domain, and the splA kinase of dictyostelium and rabbit ryanodine receptor (SPRY) domain [14,15]. Some evidence suggests that TRIM4 is overexpressed with DNA hypomethylation in hepatocellular carcinomas and is associated with poor prognosis [16]. A recent study has revealed that TRIM4 induces cisplatin resistance in osteosarcoma through an undisclosed pathway [17]. However, the roles of TRIM4 in OC have not been characterized.

In this study, we report that TRIM4 was weakly expressed in CDK4/6is-sensitive OC organoids. Mechanistically, we demonstrate that TRIM4 binds to and ubiquitinates hnRNPDL to activate CDKN2C. Furthermore, we confirm that hnRNPDL degrades CDKN2C mRNA in OC. We also observe a negative correlation between TRIM4 expression and both hnRNPDL and CDK4/6 expression levels in clinical specimens. Collectively, our findings suggest that targeting CDK4/6 inhibitors might be effective for treating OC patients with low levels of TRIM4.

Materials and methods

Clinical specimens

A paraffin tissue microarray comprising 74 high-grade serous OC (HGSC) samples and 10 normal samples from patients undergoing operations at Ruijin Hospital from July 2018 to January 2022 was used. Fifteen HGSC specimens were obtained from patients who underwent surgery at Ruijin Hospital from October 2022 to February 2023 and were used to establish organoid models.

Cell lines and reagents

The HEK293T (RRID:CVCL_0063), A2780 (RRID:CVCL_0134), OVCAR-3 (RRID:CVCL_0465), HEY (RRID:CVCL_0297), OVCA433 (RRID:CVCL_0475), SKOV-3 (RRID:CVCL_0532) cell lines were purchased from Fuheng Biotech, China. HEK293T cells were maintained in DMEM (Gibco, USA), and the other cell lines were maintained in RPMI-1640 medium (BioAgrio, China) containing 10% fetal bovine serum (Gibco) and 1% penicillin–streptomycin (Gibco) in a humidified incubator containing 5% CO_2 at 37 °C. All cell lines were authenticated using short tandem repeat (STR) profiling within the last three years. All experiments were performed with mycoplasma-free cells. Cell viability was determined using the Cell Counting Kit-8 (CCK-8, Dojindo, Japan) assay. TQB3616 was obtained from Chia Tai Tianqing Co., Ltd. (China).

Organoid cultures and assays

For culturing organoids, primary tumor tissues were cut into small fragments (< 1 mm), and a single-cell suspension was prepared by enzymatic digestion, shaking and filtration through a 100 μm filter. The single-cell suspension was mixed with Matrigel (Yeason, China), plated into a 24-well plate and solidified in an incubator for 30 min. Ovarian Cancer Organoid Medium (BioGenous, China) containing the necessary cytokines and recombinant proteins was then added to each well.

For drug screening, cultured OC organoids with a diameter of approximately 50 μm were collected and plated into 96-well plates as previously described [18]. Serially diluted TQB3616 or DMSO was added to triplicate wells. After 72 h, the medium was removed, and organoid viability was tested with a Cell Counting Lite 3D Luminescent Cell Viability Assay (Vazyme, China). The half-maximal inhibitory concentration (IC_{50}) was then calculated. The rest of each sample was stored in RNAfollow (NCM Biotech, China) until RNA sequencing was performed.

RNA sequencing analysis

An Agilent 2100 Bioanalyzer (Agilent Technologies, Inc.) was used to measure the RNA concentration, RIN value, 28S/18S ratio and fragment size to determine RNA integrity. Total RNA (1 μg) was used for subsequent library preparation. We filtered the low-quality reads (the quality of more than 20% of the bases was lower than 10), reads with adaptors, and reads with unknown bases (more than 5% N bases) to obtain the clean reads. Gene counts were normalized and analyzed using the DESeq2 method. Volcano plots were used to estimate the differential expression of genes in the samples.

Plasmid construction and transfection

Human full-length TRIM4 was cloned and inserted into pcDNA3.1 (LncBio Co., Shanghai, China). TRIM4 and hnRNPDL siRNAs were designed by LncBio Co. (Shanghai, China), and the sequences are provided in Table S1. siRNA and plasmids were transfected into SKOV-3 cells following incubation for 48 h.

Western blotting and immunoprecipitation

Total protein was extracted from cells using RIPA lysis buffer (New Cell & Molecular Biotech, Suzhou, China) containing PMSF (Biosharp, Hefei, China), and the protein concentration was quantified by the BCA assay (Biosharp). The samples were separated by 10% SDS polyacrylamide gel electrophoresis and transferred to membranes, which were blocked with 5% nonfat milk. Then, the membranes were probed with one of the following primary antibodies: anti-ubiquitin (Cell Signaling Technology (CST), 3936, 1:1000), anti-DYKDDDDK Tag (CST, 14793, 1:1000), anti-Myc-Tag (CST, 2276, 1:5000), anti-TRIM4 (Sino Biological, 204421, 1:1000), and anti-hnRNPDL (ABclonal, A10721, 1:1000). For the IP assay, total protein lysates were incubated overnight at 4 °C with the following primary antibodies: anti-DYKDDDDK Tag, anti-Myc-Tag, anti-TRIM4, and anti-hnRNPDL (ABclonal, A10721, 1:20). They were then incubated with Magnetic Bead Conjugated IgG (mouse mAb, Cell Signaling Technology, Cat No. 5873, 1:20). Then, protein A/G agarose beads (Thermo Fisher Scientific) were added for 3–4 h before extensive washing with RIPA buffer. The bands were visualized via an electrochemiluminescence imaging system (Tanon, China) and analyzed using ImageJ (Fiji).

GST pull-down

The recombinant TRIM4-GST and hnRNPDL-His vector were introduced into *Escherichia coli*. Protein expression was assessed using SDS-PAGE and Coomassie bright blue staining, facilitated by Zoonbio Biotech, Nanjing. The enriched protein was then incubated with GST Magarose Beads (BersinBio, Guangzhou, China) at 4 °C for 4 h. Subsequently, the mixture was subjected to Western blotting using primary antibodies, including anti-GST (Zoonbio, 1:1000) and anti-His (Zoonbio, 1:4000). The resulting bands were probed with a secondary antibody and visualized using electrochemiluminescence imaging (Tanon, China).

Real-time quantitative PCR (RT-qPCR) analysis

Total RNA was extracted using TRIzol reagent (Thermo Fisher Scientific, USA). Reverse transcription and RT-qPCR were performed using the BeyoRT Kit and qPCR mix Kit (Beyotime Biotech, China). The relative mRNA levels of genes were normalized to the expression of GAPDH and calculated using the 2-ΔΔCT method. All primers used were synthesized by BioTNT, and their sequences are provided in Table S1.

RNA immunoprecipitation (RIP)

We performed RIP with an anti-hnRNPDL antibody according to the instructions of the RIP kit (BersinBio, Guangzhou, China). Cells were collected and lysed with RIP lysis buffer, and then 50 μL of magnetic beads conjugated with anti-IgG antibodies were added. The mixture was incubated overnight at 4 °C with rotation. Then, the supernatant was purified, and RNA was extracted for RT-qPCR.

Mass spectrometry

Liquid chromatography-tandem mass spectrometry (LC-MS) was performed by Novogene (Beijing, China) as previously described [19]. The detailed procedures are provided in the supplementary data.

Tissue microarray (TMA) staining

IHC was performed on formalin-fixed tissue microarrays containing 74 HGSC and 10 normal specimens from patients at Ruijin Hospital. IHC staining was conducted with primary antibodies against CDK4 (Bioss, 52028, 1:200), CDK6 (Bioss, 0568, 1:200), TRIM4 (ABclonal, A15922, 1:200), hnRNPDL (Bioss, 17343, 1:300), and CDKN2C (rabbit pAb, Bioss, Cat No. 4270, 1:200). The expression level of each target protein was quantified by 2 pathologists blinded to the clinical conditions and assessed using the modified H-score ([{% of weak staining} × 1] + [{% of moderate staining} × 2] + [{% of strong staining} × 3]) [20]. Pearson product-moment correlation analysis was used to estimate correlations

among target protein expression (r = correlation coefficient).

Flow cytometry analysis

After treatment, cells were collected and permeabilized with cold 75% ethanol overnight at −20 °C. Then, the cells were incubated with RNase I (10 μg/mL) in PBS at 37 °C for 30 min and stained with propidium iodide (50 μg/mL) for 15 min at room temperature. The proliferation index (PI) was calculated to evaluate the percentage of cells in proliferative phases according to the following formula:

$$PI = \frac{S + \frac{G2}{M}}{\frac{G0}{G1} + S + \frac{G2}{M}}$$

For the apoptosis assay, cells were stained with an Alexa Fluor 488 Annexin V/Dead Cell Apoptosis Kit (Thermo Fisher Scientific). Briefly, samples were resuspended in 1× annexin binding buffer and incubated with 5 μL Annexin V-PE (phycoerythrin) and 5 μL 7-AAD (7-amino-actinomycin) at room temperature for 15 min in the dark. All samples were subjected to flow cytometry (Beckman Coulter, Miami, FL, USA) and analyzed with FlowJo software.

Ovarian cancer subcutaneous tumor model

To establish a subcutaneous tumor model of ovarian cancer, female BALB/c nude mice (4–5 weeks old) obtained from Shanghai Lingchang Biology Co., LTD, China, were housed in a specific pathogen-free environment at Shanghai Jiao Tong University School of Medicine. The animal license number for this experiment is SYXK 2018–0027. The mice were randomly assigned to four groups (n = 6 per group) and were inoculated with SKOV-3 cells. A total of 2×10^6 cells were injected intraperitoneally into the mice along with matrigel. Following a complete 28-day administration period, the mice were euthanized and the tumors were collected, quantified, and visually documented. Tumor tissue and samples from affected organs were preserved in a 4% paraformaldehyde solution, subsequently embedded in paraffin, and subjected to sectioning and staining with hematoxylin and eosin (H&E). The resulting slides were evaluated using a Digital Pathology Slide Scanner (KF-PRO-120, KFBIO, China).

Statistical analysis

All analyses were performed in triplicate in 3 independent experiments. IBM SPSS 22.0 software (SPSS Inc., Chicago, IL, USA) and GraphPad Prism software (Version 6.01, GraphPad Software, Inc., USA) were used for data analysis. The results are presented as the mean ± SD. The significance of differences was determined by Student's t-tests unless otherwise stated. Survival rates were assessed using Kaplan–Meier analysis. Numerical data were evaluated using the χ^2 test or Fisher's exact probability test. A P value < 0.05 was considered to indicate statistical significance.

Availability of data

Next-generation sequencing data and clinical data from The Cancer Genome Atlas (TCGA) and International Cancer Genome Consortium (ICGC) were obtained and analyzed via ACLBI. The splicing RNA-seq data from the cell line used were obtained from an article published by Li *et al*. [21]. The RNA-seq data reported in this paper have been deposited in the OMIX, China National Center for Bioinformation/Beijing Institute of Genomics, Chinese Academy of Sciences under accession number OMIX005044. The mass spectrometry data generated in this study have been deposited in the OMIX database under accession number OMIX005043. Further information is available from the corresponding author upon request.

Results

TRIM4 is a predictive marker of the response to CDK4/6i in ovarian cancer, and its expression is inversely correlated with CDK4/6 expression

To explore potential genes that may modify the effect of CDK4/6is, we initially established 15 patient-derived OC organoid models (Fig. 1A and 1B). A portion of each sample was utilized to evaluate the efficacy of TQB3616, a novel CDK4/6i currently undergoing clinical trials. The remaining tissue was then subjected to RNA-seq analysis (Fig. 1A). The IC_{50} values of TQB3616 ranged from 9.7 to 2200 nmol/L, with the median value used as a cut-off point for grouping the organoids. Specifically, organoids with IC_{50} values above the median were categorized into the "poor response" group (n = 8), while those below were included in the "good response" group (n = 7).

RNA-seq analysis of organoid-derived tissues treated with TQB3616 revealed 319 upregulated genes and 363 downregulated genes in the poor response group compared with the good response group (Fig. 1C and 1D). GO enrichment analysis of upregulated genes identified several protein ubiquitination genes in the gene ontology (GO) database (GO: 0016567), which includes *TRIM4*, *CAND1*, *TRIM33*, *RNF11*, and *NEDD4* (Fig. 1C). Notably, TRIM4 exhibited the most significant upregulation with a $\log_2$(fold change) value of 10.7 and P-value of 0.005, hence, we focus on TRIM4.

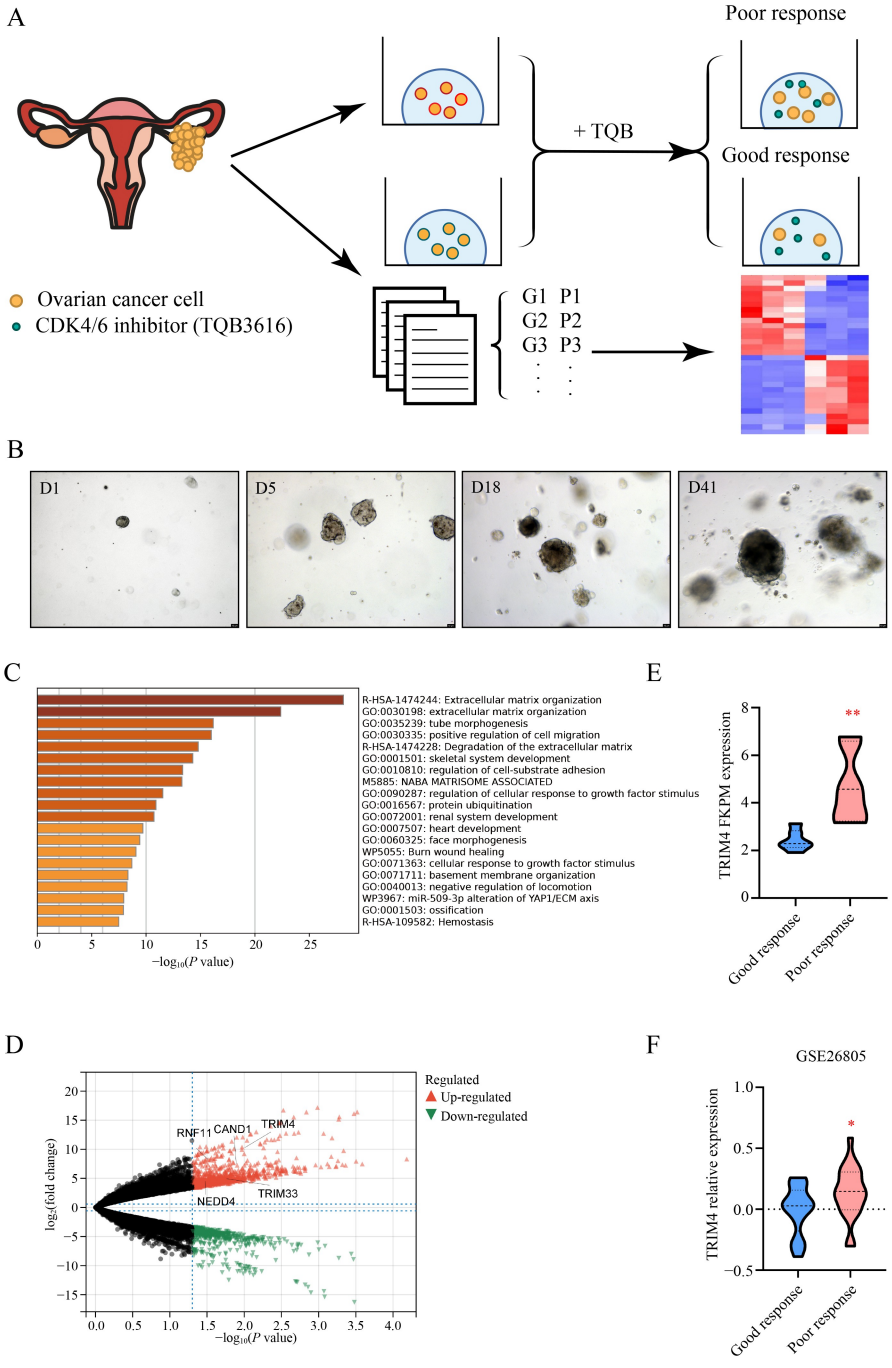

Fig. 1 TRIM4 is a predictive marker of CDK4/6i response in ovarian cancer. (A) Overview of the study design. After the acquisition of ovarian cancer tissue, the major part was used to develop patient-derived organoids and went over the drug resistance test of TQB3616 to divide into two subgroups with poor or good response. The rest part was used for RNA-seq. (B) Representative serial images of ovarian cancer organoids at the indicated times (day 1, day 5, day 18, day 41). Scale bar, 10 μm. (C) GO enrichment analysis of upregulated genes in OC tissue. (D) Differential expressed genes between poor versus good response group to TQB3616. (E and F) Relative TRIM4 expression in the OC tissue (E) and cell lines (F) from subgroups with poor response and good response to TQB3616. *$P < 0.05$, **$P < 0.01$.

Furthermore, we observed that OC samples exhibiting a poor response to TQB3616 displayed higher levels of TRIM4 ($P = 0.003$) (Fig. 1E). We also examined the TRIM4 expression levels in 40 OC cell lines with diverse responses to CDK4/6 inhibitors in GSE26805 data set [7] and found significantly increased TRIM4 expression in cells showing poor response to CDK4/6is ($P = 0.038$) (Fig. 1F).

Subsequently, we investigated the potential correlation between TRIM4 and CDK4/6 expression. By utilizing of the International Cancer Genome Consortium (ICGC) and The Cancer Genome Atlas (TCGA) databases, we

discovered that TRIM4 expression level in ovarian cancer patients had an inverse correlation with that of CDK4 and CDK6 (ICGC, R = −0.37, $P < 0.001$; TCGA, R = −0.18, $P = 0.02$) (Fig. S1A and S1B). Secondly, we examined the expression of TRIM4 and CDK4/6 in a tissue array consisting of 74 OC tumor tissues and 10 normal ovarian tissues (the clinicopathologic features of the patients are detailed in Table S2). According to the H-score analysis, TRIM4 expression was significantly higher in the tumor group than in the normal group ($P < 0.05$) (Fig. S1C). The percentage of patients with high TRIM4 expression levels was greater in the tumor group than in the normal group (89.2% vs. 37.5%, $P < 0.05$) (Fig. S1D). Furthermore, we observed that tumor tissues with low TRIM4 expression exhibited elevated levels of CDK4 and CDK6 expression ($P < 0.001$) (Fig. S1F–S1G). These findings suggest an inverse correlation between TRIM4 expression and CDK4/6 expression, sensitivity to TQB3616.

Decreased TRIM4 expression enhances the sensitivity to TQB3616 in an OC cell line

Generally, CDK4/6is induce cell cycle arrest in G0–G1 phase, thereby preventing cells from entering subsequent phases. To elucidate the mechanisms by which TRIM4 suppresses the effects of TQB3616, we investigated cell cycle progression and the apoptosis rates in SKOV-3 cells with a relatively high intrinsic TRIM4 expression level and a relatively low CDK4/6 expression level (Figs. 2A, S2A, and S2B).

As expected, TQB3616 treatment increased the proportions of cells in G1 phase (Fig. 2D) and apoptotic cells (Fig. 2E). Overexpression of TRIM4 elevated the proportion of cells in S phase and consequently increased PI (Fig. 2B–2D). When TQB3616 was administered to cells overexpressing TRIM4 at a concentration of 500 nmol/L, there was an increase in PI and a decrease in apoptotic cell percentage compared with TQB3616 treatment alone, indicating that high TRIM4 expression weakened the effect of TQB3616. As shown in Fig. 2D, si-TRIM4 did not alter PI or apoptotic cell proportion. At the same time, TRIM4 did not affect the growth rate of ovarian cancer cells (Fig. S2C). However, silencing TRIM4 combined with TQB3616 treatment (500 nmol/L) resulted in decreased PI and increased apoptotic cell proportion compared with sole administration of TQB3616 (Fig. 2D and 2E). These findings suggest that TRIM4 partially counteracts the ability of TQB3616 to induce apoptotic cell death and reduce OC cell proliferation.

TRIM4 expression is inversely associated with hnRNPDL expression

Given that TRIM4 functions as an E3 ligase, we hypothesized that it exerts its effects by modulating a specific protein substrate. We conducted immunoprecipitation (IP) and LC-MS analysis on TRIM4-overexpressing HEK293T cells to identify the proteins directly binding to TRIM4. Our results revealed 97 upregulated proteins out of a total of 751 differentially expressed proteins that exhibited a strong association with TRIM4 (Fig. 3A). GO enrichment analysis indicated that these TRIM4 binding proteins were primarily involved in the mRNA splicing-major pathway (Fig. 3B), with heterogenous ribonuclear protein D-like (hnRNPDL) showing the strongest binding affinity for TRIM4 binding (Fig. 4C). Additionally, we employed a tissue microarray to validate the correlation between TRIM4 and hnRNPDL expression. The findings demonstrated a negative relationship between the two proteins, supported by an R-value of −0.32 (Fig. 3D and 3E). Based on these observations, we postulated that hnRNPDL serves as the substrate of TRIM4. However, in SKOV-3 cells overexpressing TRIM4, no significant difference was observed in the relative mRNA level of hnRNPDL; conversely, there was a notable decrease in the protein level compared to the control group (Fig. 3F and 3G). Overall, our hypothesis suggests that TRIM4 regulates hnRNPDL expression at the post transcriptional level.

TRIM4 directly binds to hnRNPDL and promotes its ubiquitin-mediated degradation

We conducted a co-IP assay to assess the potential interaction between TRIM4 and hnRNPDL. In HEK293T cells, overexpressed TRIM4 was found to bind to hnRNPDL (Fig. 4A). Endogenous co-IP experiments further confirmed the binding of TRIM4 and hnRNPDL in SKOV-3 cells (Fig. 4B). To demonstrate the direct interaction between TRIM4 and hnRNPDL *in vitro*, we performed GST pull-down assay with recombinant GST-TRIM4 and His-hnRNPDL. The GST blot showed a successful pulldown of both GST and GST-TRIM4, consistent with the co-IP results (Fig. 4C). Previous studies have identified four conserved domains of TRIM4 [22]. To determine which specific domain interacts with hnRNPDL, we generated four truncation mutants, TRIM4ΔRING, TRIM4ΔB-box, TRIM4ΔCC, and TRIM4ΔSPRY. These mutants were then co-transfected with FLAG-hnRNPDL into HEK293T cells (Fig. 4D). A coimmunoprecipitation assay revealed that wild-type TRIM4, as well as the ΔRING variants, interacted with hnRNPDL; however, no interaction was observed between hnRNPDL and ΔSPRY, ΔCC or the ΔB-box variant of TRIM4 (Fig. 4E). Furthermore, we investigated whether TRIM4 regulates the stability of hnRNPDL or accelerates hnRNPDL degradation. Our results demonstrated that ectopic expression of TRIM4 in SKOV-3 cells treated with MG132, a proteasome

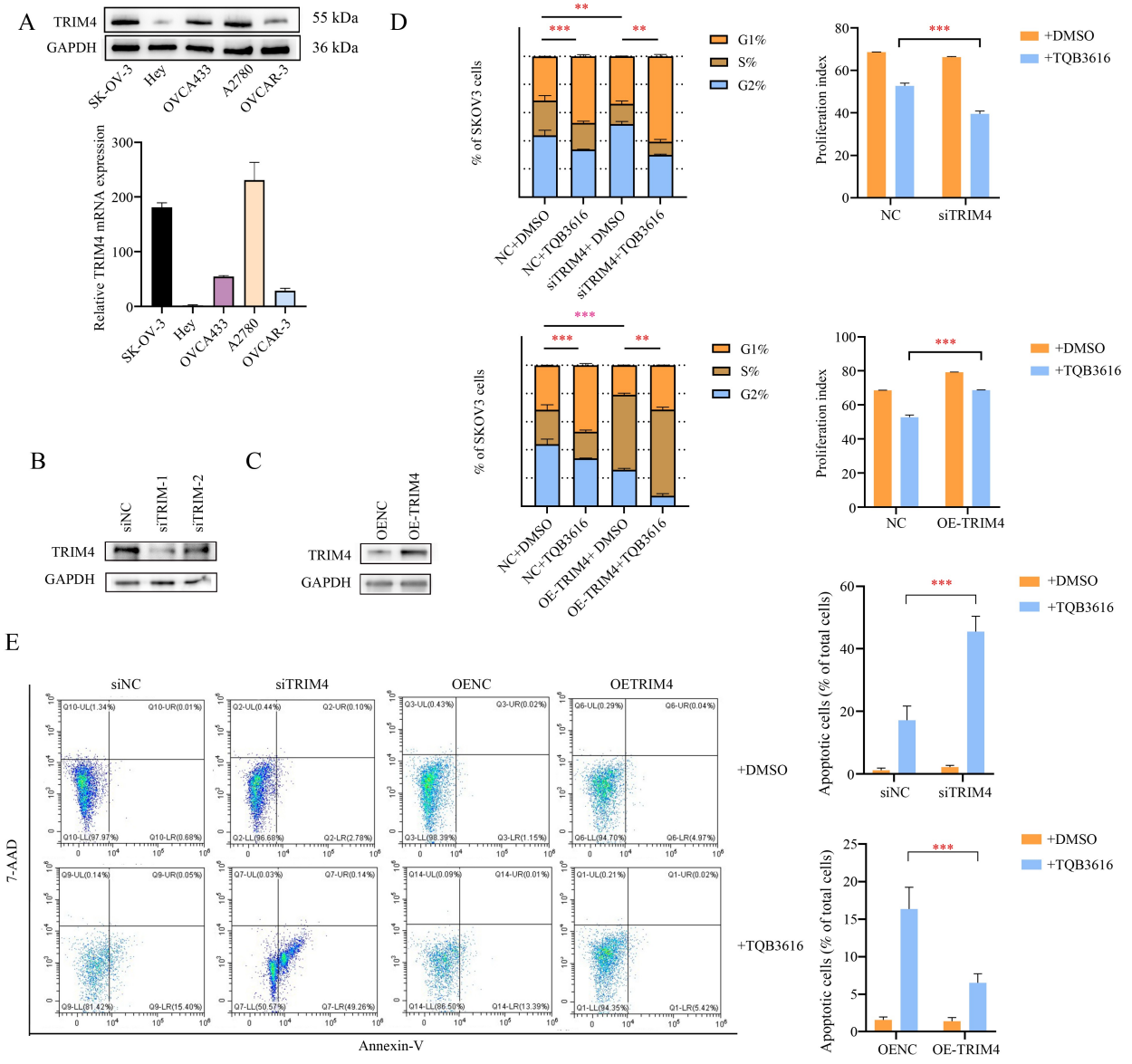

Fig. 2 TRIM4 expression affects sensitivity to TQB3616 in SKOV-3. (A) Protein and mRNA levels of TRIM4 in ovarian cancer cell lines. (B) The efficacy of TRIM4 siRNA. (C) The efficacy of TRIM4 overexpression. (D) Cell-cycle analysis and PI analysis of cell si-TRIM4 and OE-TRIM4 with and without treatment of TQB3616 (500 nmol/L, 24 h). (E) Apoptosis assay of cell si-TRIM4 and OE-TRIM4 with and without treatment of TQB3616 (500 nmol/L, 24 h). $^{**}P < 0.01$, $^{***}P < 0.001$.

inhibitor, increased ubiquitination level on hnRNPDL (Fig. 4F). These findings collectively confirm that TRIM4 interacts with hnRNPDL through its RING and B-box domains to facilitate hnRNPDL ubiquitylation and degradation.

hnRNPDL regulates the expression of CDKN2C through alternative splicing

Belonging to the heterogeneous nuclear ribonucleoprotein (hnRNP) family, hnRNPDL is primarily recognized as an intronic/exotic splicing silencer (ISS and ESS). To elucidate the splicing targets of hnRNPDL, Li *et al*. [22] conducted a transcriptome-wide study in hnRNPDL-knockdown HeLa cells. By analyzing their publicly available RNA-seq data, we discovered an upregulation in the expression of cell cycle-related genes, with cyclin-dependent kinase inhibitor 2 (CDKN2C) exhibiting the highest expression level. As demonstrated in their study, CDKN2C interacts with CDK4/6 to inhibit the formation of the cyclin D-CDK4/6 complex, thereby impeding cell cycle progression [23]. Therefore, we hypothesized that hnRNPDL participates in the degradation of CDKN2C mRNA (Fig. 5A). For our mRNA studies, two qRT-PCR primer sets were designed for CDKN2C spanning, with two different exon–exon junctions, as shown in Fig. 5A.

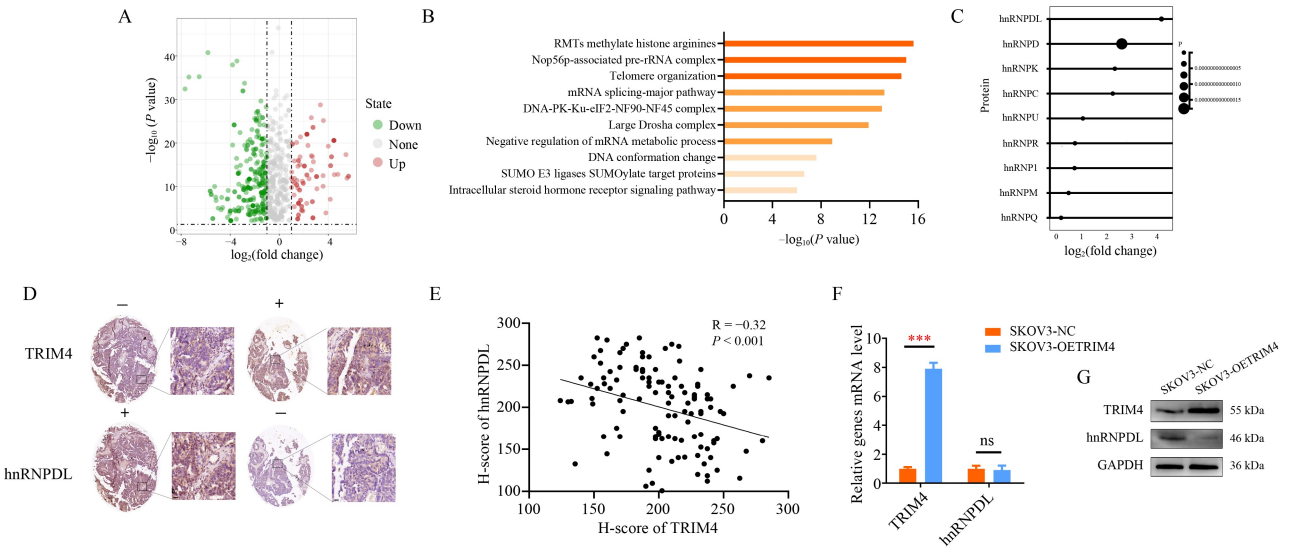

Fig. 3 TRIM4 expression is inversely associated with hnRNPDL. (A) The volcano plot of proteins interacting with TRIM4. (B) GO enrichment analysis of upregulated proteins in proteomics. (C) The bubble plot of proteins enriched in mRNA splicing-major pathway. (D) IHC analysis of TRIM4 and hnRNPDL in OC tissue microarray. Scale bar, 10 μm. (E) The correlation between the H-score of TRIM4 and hnRNPDL. (F) mRNA expression of hnRNPDL in OE-TRIM4 SKOV-3 cells. (G) Protein levels of TRIM4 and hnRNPDL in SKOV-3 cells. ns, not significant. ***$P < 0.001$.

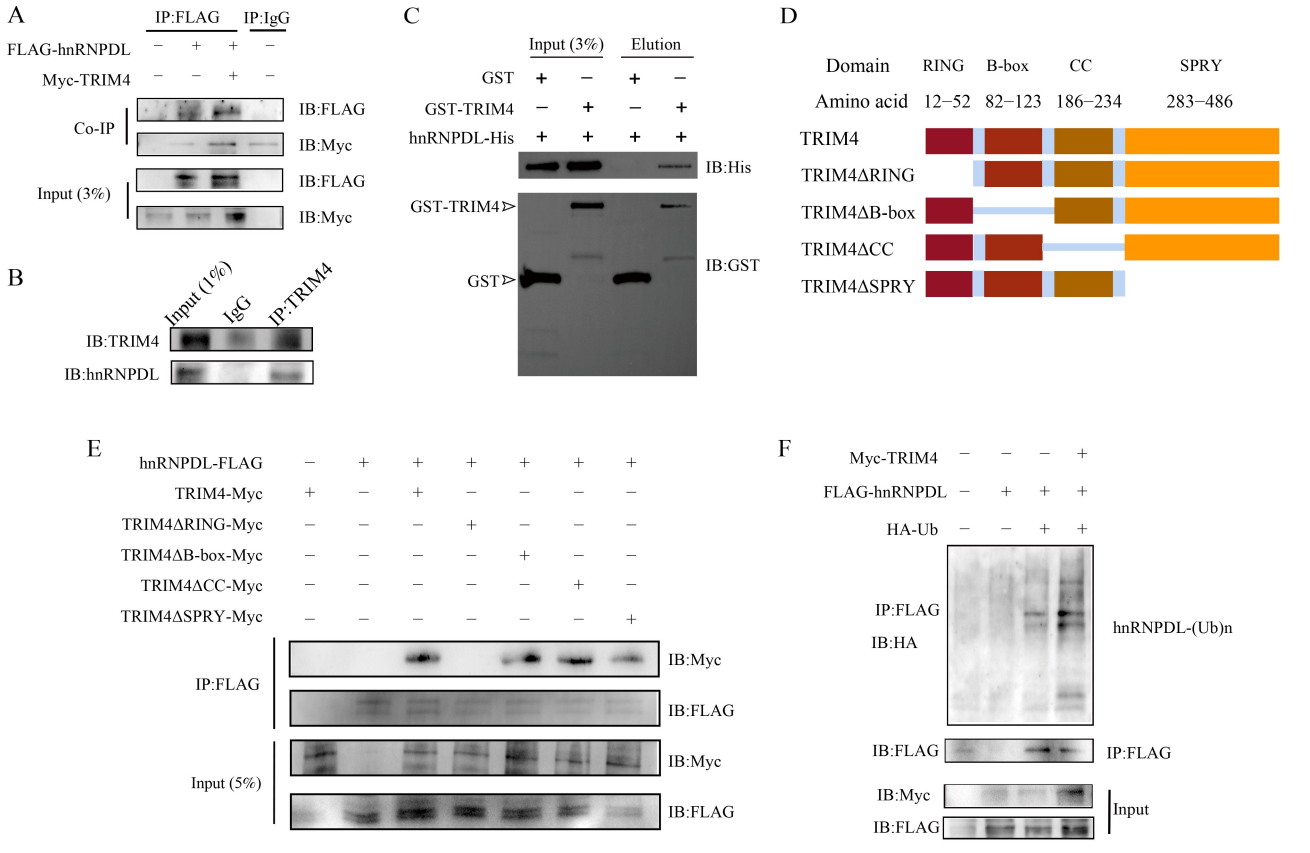

Fig. 4 TRIM4 directly binds to hnRNPDL and promotes its ubiquitin-mediated degradation. (A) Coimmunoprecipitation assay of TRIM4 and hnRNPDL in HEK293T cells transfected with FLAG-tagged hnRNPDL and Myc-tagged TRIM4. (B) Coimmunoprecipitation assay of TRIM4 and hnRNPDL in SKOV-3 cells. (C) GST pull-down assay of GST-TRIM4 and hnRNPDL-His. (D) Schema of the structural domains of TRIM4. (E) Coimmunoprecipitation assay of TRIM4 and hnRNPDL in HEK293T cells transfected with sequential segments of TRIM4 plasmids. (F) Coimmunoprecipitation ubiquitination assay of ubiquitinated hnRNPDL using SKOV-3, cells transfected with FLAG-tagged hnRNPDL, Myc-tagged TRIM4 and/or HA-tagged ubiquitin and treated with MG132 (20 mmol/L, 6 h).

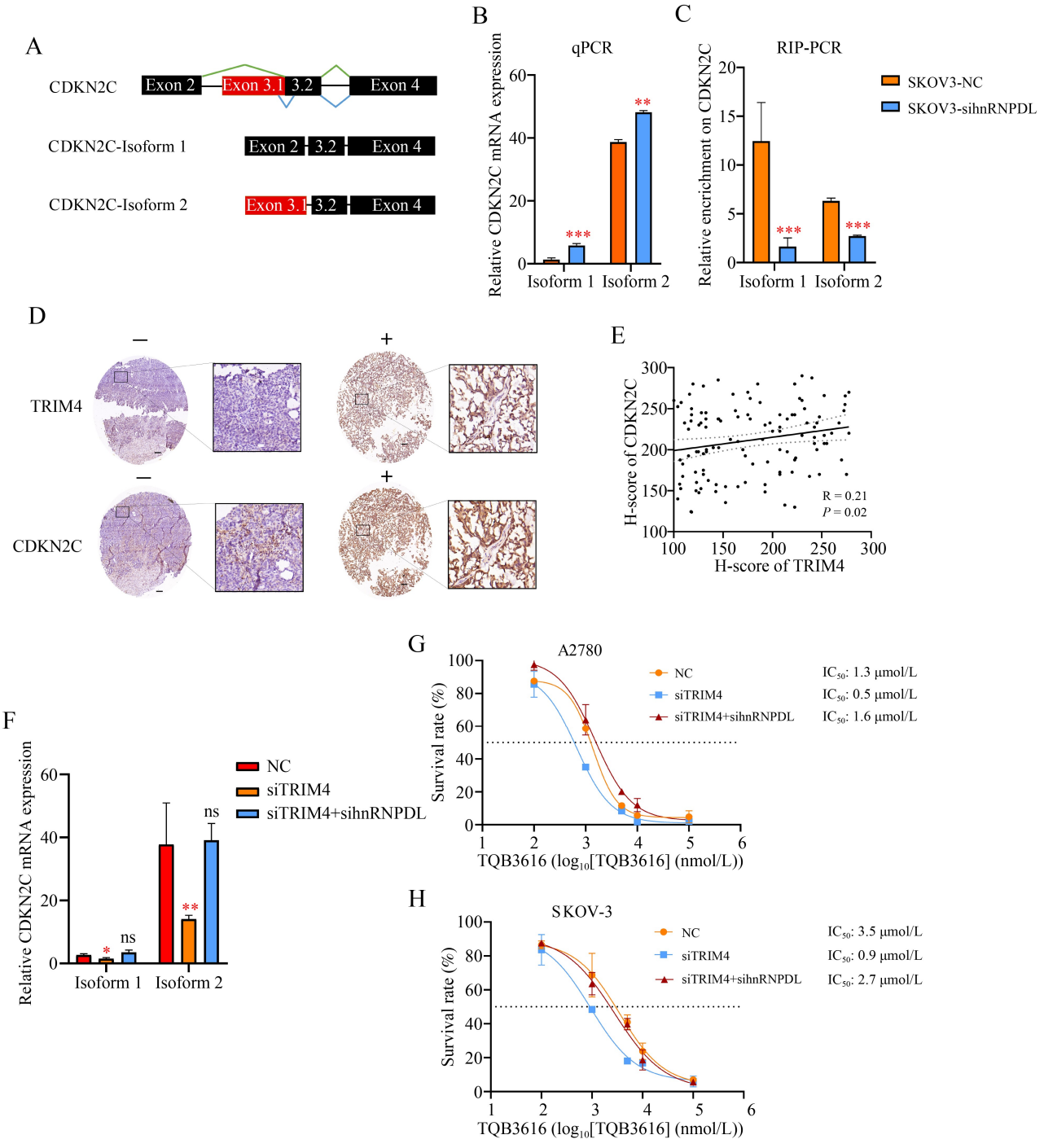

Fig. 5 hnRNPDL regulates CDKN2C expression through alternative splicing. (A) Alternative splicing mechanisms of CDKN2C, colorful lines show two bridge strategies, including exon 2–exon 3.2–exon 4 (isoform 1, black) and exon 3.1–exon 3.2–exon 4 (isoform 2, red). (B and C) Relative mRNA expression (B) and relative enrichment (C) of CDKN2C isoform 1 and CDKN2C isoform 2 in SKOV-3 cells transfected with siRNA of hnRNPDL. (D) IHC analysis of TRIM4 and CDKN2C in OC tissue microarray. Scale bar, 10 μm. (E) The correlation between the H-score of TRIM4 and CDKN2C. (F) Relative mRNA expression of CDKN2C isoform 1 and isoform 2 in SKOV-3 cells following transfection with either siRNA targeting TRIM4 alone or in combination with siRNA targeting both TRIM4 and hnRNPDL. (G and H) The drug sensitivity of TQB3616 was assessed in A2780 cells (G) and SKOV-3 cells (H) following transfection with either siRNA targeting TRIM4 alone or in combination with siRNA targeting both TRIM4 and hnRNPDL.

We performed PCR analysis of SKOV-3 cells and observed an increase in the levels of both the inclusion isoform transcript (isoform 1) and skipping isoform transcript (isoform 2) of CDKN2C in cells transfected with si-hnRNPDL (Fig. 5B). Subsequently, RIP experiments were conducted to evaluate the binding

between the hnRNPDL protein and CDKN2C transcripts. RIP results indicated weaker binding between both CDKN2C isoforms and hnRNPDL protein due to reduced levels of hnRNPDL expression (Fig. 5C). The combined findings from RIP analysis and data on CDKN2C isoform mRNA levels suggest that hnRNPDL binds to CDKN2C isoform 2 and suppresses its expression. The correlation between TRIM4 and CDKN2C expression was also assessed using clinical specimens TMA as previously described. Fig. 5D and 5E demonstrates a positive correlation between TRIM4 and CDKN2C expression (P = 0.02). Endogenous TRIM4 downregulates hnRNPDL expression leading to alleviation of repression of CDKN2C translation.

To confirm these findings, we conducted transfection experiments with si-TRIM4 and si-hnRNPDL to restore the expression of CDKN2C. We observed a significant reduction in CDKN2C expression levels upon silencing TRIM4 alone. However, when hnRNPDL was also silenced, the expression level of CDKN2C was restored to a level comparable to that in the control group (Fig. 5F). Additionally, knockdown of TRIM4 increased cell sensitivity to TQB3616, whereas simultaneous silencing of both TRIM4 and hnRNPDL normalized the IC_{50} of TQB3616 (Fig. 5G and 5H).

siTRIM4 and CDK4/6i synergistically attenuates the growth of ovarian tumor *in vivo*

To systematically evaluate the *in vivo* impact of TRIM4 on OC, we conducted an experiment using siRNA administration and the jetPEI delivery system approved by FDA for OC treatment. In this study, to maintain a higher bioavailability, an evaluation was conducted on three modified versions of siTRIM4 in an *in vivo* setting. Notably, the modified siTRIM4 incorporating advanced enhanced stabilization chemistry (ESC), referred to as DV22, exhibited a remarkable efficacy in suppressing TRIM4 expression *in vivo* (Fig. S3A). Female BALB/c nude mice were randomly allocated into four groups receiving saline as control, intra-tumoral injection of modified siTRIM4, administration of TQB3616, or a combined treatment involving siTRIM4 and TQB3616. Following a 25-day administration period, the mice were sacrificed according to the protocol outlined in Fig. 6A. Notably, the tumor weight of mice subjected to the combined treatment of siTRIM4 and TQB3616 exhibited a significantly reduced weight compared with the other experimental groups (Fig. 6B and 6C), with lowest tumor size observed in those receiving combination treatment while those receiving TQB3616 alone progressed slower than siTRIM4 group (Fig. 6D and 6E). Histological examination demonstrated a significant decrease in TRIM4 expression and an increase in CDK4/6 expression in the treatment group subjected to siTRIM4 (Figs. 6F and S3B). Collectively, these findings provide evidence that TRIM4 hinders the splicing activity of hnRNPDL through ubiquitylation, thereby preventing the suppression of CDKN2C expression, ultimately leading to an inadequate response to TQB3616 (Fig. 6G).

Discussion

Elucidating the functional effects of CDK4/6is is crucial for developing effective therapeutic strategies for ovarian cancer. In this study, we have discovered that TRIM4, an E3 ligase, plays a critical role in regulating the sensitivity of OC cells to the CDK4/6 inhibitor TQB3616. Specifically, TRIM4 targets hnRNPDL for ubiquitination and subsequent proteasomal degradation, thereby modulating CDKN2C expression through splicing regulation and ultimately reducing the therapeutic efficacy of CDK4/6 inhibitors in ovarian cancer. These findings provide novel mechanistic insights into the sensitivity of ovarian cancer cells to CDK4/6 inhibitors and offer potential therapeutic implications.

Surprisingly, our study reveals distinct suppressive effects exerted by TQB3616, a small-molecule inhibitor of CDK4/6, in OC. A first-generation CDK4/6 inhibitor (palbociclib) was tested in 30 patients with OC and demonstrated a prolonged median PFS of 3.7 months with good tolerability [24]. Similarly, another trial showed stable disease in 50% of estrogen receptor-positive endometrial and OC patients [25] treated with ribociclib (a CDK4/6 inhibitor) combined with letrozole. Based on these phase II data, clinical trials are currently underway to evaluate the use of CDK4/6 inhibitors in OC patients. However, due to the complex and highly heterogeneous nature of OC, it is essential to identify specific patient populations who would benefit from treatment with CDK4/6 inhibitors. To address this issue comprehensively, we established organoids derived from patient specimens as an *ex vivo* model system for evaluating the sensitivity of OC organoids to TQB3616 treatment, and identified TRIM4 as a predictive marker indicating responsiveness toward TQB3616.

TRIM4 is a member of the TRIM family, a superfamily characterized by the highly conserved motif in the N-terminal region. This motif consists of a conserved RING domain, one or two B-box domains and a CC domain. Owing to their RING domain, most members of the TRIM family possess Ub-ligase activity. Additionally, several TRIM proteins have been implicated in oncogenesis and chemoresistance across various types of cancer [26,27]. For instance, TRIM37 activates the NF-κB pathway through its interaction with PDZ binding protein (PBK) in ovarian cancer, leading to resistance against olaparib, a PARP inhibitor [28]. Unlike other members of the TRIM family, limited studies have explored the role of TRIM4, let alone its role in

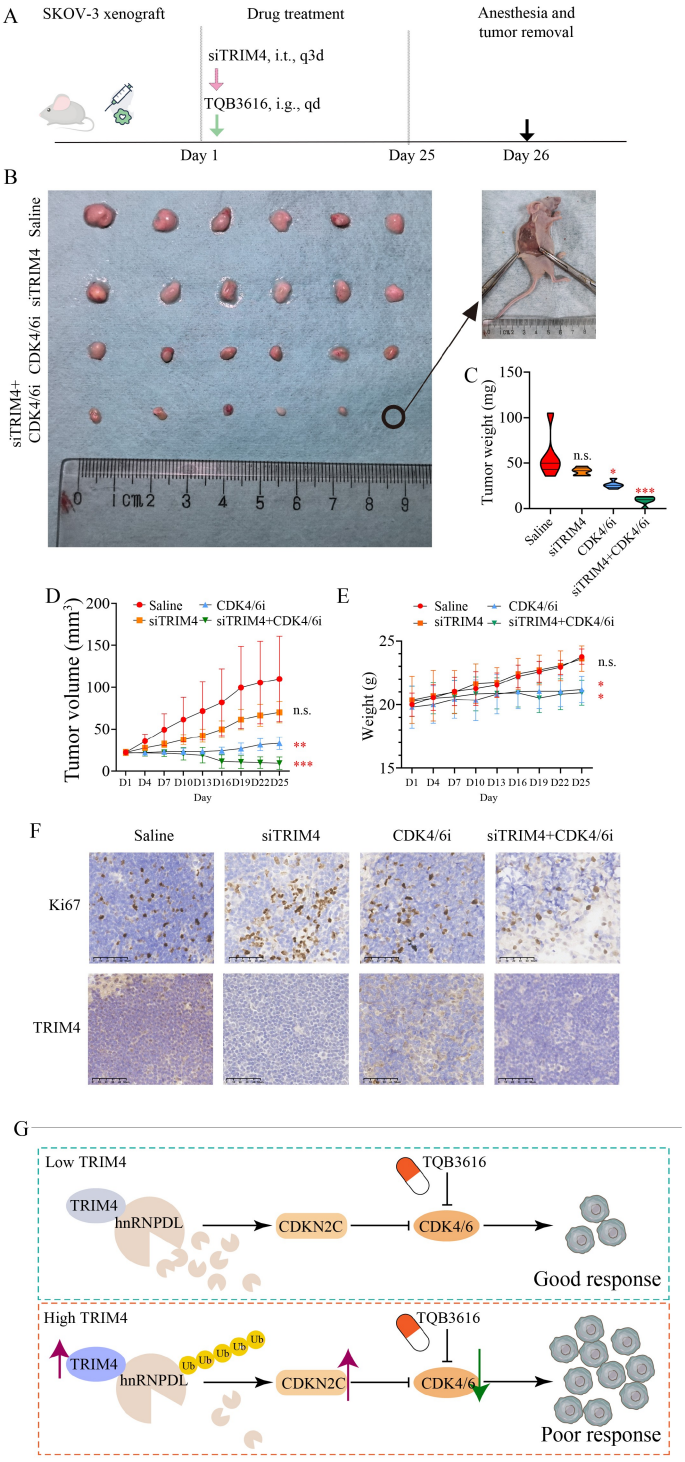

Fig. 6 siTRIM4 and CDK4/6i synergistically attenuates ovarian tumor *in vivo*. (A) Overview of the *in vivo* study design. After the subcutaneous tumor formation in one week, DV22-modified siTRIM4 (2OD) with jetPEI delivery system was intratumoral injected per 3 days and TQB3616 (10 mg/kg) was administrated every day. Following a 25-day administration period, the nude mice were sacrificed. (B) Xenograft tumors at endpoints were removed at day 26. (C) Tumor weight of nude mice underwent siTRIM4 and TQB3616 administration at day 26. (D and E) Tumor volume (D) and mice weight (E) were measured every 3 days. (F) Expression of Ki67 and TRIM4 in xenograft tumor in nude mice underwent siTRIM4 and TQB3616 administration. Scale bar, 10 μm. (G) Proposed model for the article. Briefly, high TRIM4 level drives to deactivation of hnRNPDL via ubiquitylation, thus releasing the expression of CDKN2C, which inhibits CDK4/6 and leads to a poor response toward TQB3616, as its targets are reduced. Otherwise, the loss of TRIM4 is correlated with a high sensitivity to TQB3616. $N = 6$ biological replicates. i.t., intratumoral injection; i.g. imperial gallon; ns, not significant. $^{*}P < 0.05$, $^{**}P < 0.01$, $^{***}P < 0.001$.

carcinoma. However, it has been identified as a positive regulator of virus-triggered interferon (IFN) by targeting retinoic acid-inducible gene 1 (RIG-1) [29,30]. Furthermore, TRIM4 has been found to interact with peroxiredoxin 1 during oxidative stress and with TRPM8 during allodynia. Structurally, TRIM4 comprises a RING domain that facilitates protein–protein interactions by forming the catalytic center along with the SYPR domain, a B-box motif that aids in target protein recognition, and a CC region responsible for homogenization within TRIM4 [31–33]. We provide evidence suggesting that hnRNPDL binding to TRIM4 is disrupted by its RING domain similar to other TRIM proteins. These findings support previous research on this specific binding region area of TRIM4 and its association with target proteins.

hnRNPDL belongs to hnRNPs subfamily responsible for the processing of heterogeneous nuclear pre-mRNA into mature mRNA and its transportation. Ruth and his team's comprehensive investigation on gene regulation following hnRNPDL depletion revealed that it regulates the expression of multiple genes [34]. hnRNPDL contains two RNA binding domains and exhibits a preference for binding with the ACUAGCA consensus, which distinguishes it from other similar hnRNPDs [35,36]. Previous studies has explored the impact of hnRNPDL on muscular dystrophy [37]. Our analysis provides insights into how TRIM4 modulates hnRNPDL using TRIM4-adsorbing cell lysates by mass spectrometry. Regretfully, we were unable to identify the specific domain of hnRNDPL that interacts with TRIM4. hnRNPDL consists of two structurally similar RNA binding domains. Truncation mutants of hnRNPDL could not be generated due to failed protein expression in HEK-293T cells and OC cells. We utilized sequencing data sets from Ruth's group and identified the intersection with cell cycle-related gene clusters. Notably, our analysis revealed CDKN2C, another endogenous suppressor of CDK4/6, as a key target of hnRNPDL whose activity is modulated by TRIM4. Mechanistically, during the G0–G1 phase, CDK4/6 activity is inhibited through binding to members of the INK4 family (CDKN2A, CDKN2B, CDKN2C, and CDKN2D). Notably, previous studies on OC have emphasized the association between CDKN2A and overall survival [38,39]. Our research provides additional evidence supporting the significance of another crucial member of the INK4 family, namely CDKN2C in OC.

In this study, we employed genomic analysis and drug sensitivity tests using organoid models to identify key genes involved in the response to CDK4/6 inhibitors in OC. Our findings unveil a novel regulatory axis involving TRIM4/RNA binding protein hnRNPDL/CDKN2C that mediates the efficacy of CDK4/6. Mechanistically, our study demonstrates that TRIM4 promotes the degradation of hnRNPDL, leading to increased expression of CDKN2C and subsequent resistance to CDK4/6i. Consequently, OC patients with low TRIM4 expression levels are more likely to exhibit deficiency in CDKN2C and may benefit from treatment with CDK4/6is. We propose a novel therapeutic strategy involving the utilization of CDK4/6is for treating OC patients.

Acknowledgements

We thank AJE for its linguistic assistance during the preparation of this manuscript. This study was funded by the National Natural Science Foundation of China (Nos. 82172601 and 82303640).

Compliance with ethics guidelines

Conflicts of interest Xiaoxia Che, Xin Guan, Yiyin Ruan, Lifei Shen, Yuhong Shen, Hua Liu, Chongying Zhu, Tianyu Zhou, Yiwei Wang, and Weiwei Feng declare no conflicts of interest.

This study was approved by the Committees for Ethical Review of Research involving Human Subjects at Shanghai Jiao Tong University School of Medicine. The study was performed in accordance with the ethical standards as laid down in the 1964 Declaration of Helsinki and its later amendments or comparable ethical standards. Informed consent was obtained from all patients for being included in the study. All institutional and national guidelines for the care and use of laboratory animals were followed.

Electronic Supplementary Material Supplementary material is available in the online version of this article at https://doi.org/10.1007/s11684-024-1103-5 and is accessible for authorized users.

References

1. Siegel RL, Miller KD, Wagle NS, Jemal A. Cancer statistics, 2023. CA Cancer J Clin 2023; 73(1): 17–48
2. Kurnit KC, Fleming GF, Lengyel E. Updates and new options in advanced epithelial ovarian cancer treatment. Obstet Gynecol 2021; 137(1): 108–121
3. Lheureux S, Gourley C, Vergote I, Oza AM. Epithelial ovarian cancer. Lancet 2019; 393(10177): 1240–1253
4. Goel S, Bergholz JS, Zhao JJ. Targeting CDK4 and CDK6 in cancer. Nat Rev Cancer 2022; 22(6): 356–372
5. Spring LM, Wander SA, Andre F, Moy B, Turner NC, Bardia A. Cyclin-dependent kinase 4 and 6 inhibitors for hormone receptor-positive breast cancer: past, present, and future. Lancet 2020; 395(10226): 817–827
6. Fry DW, Harvey PJ, Keller PR, Elliott WL, Meade M, Trachet E, Albassam M, Zheng X, Leopold WR, Pryer NK, Toogood PL. Specific inhibition of cyclin-dependent kinase 4/6 by PD 0332991 and associated antitumor activity in human tumour xenografts. Mol Cancer Ther 2004; 3(11): 1427–1438
7. Konecny GE, Winterhoff B, Kolarova T, Qi J, Manivong K, Dering J, Yang G, Chalukya M, Wang HJ, Anderson L, Kalli KR, Finn RS, Ginther C, Jones S, Velculescu VE, Riehle D, Cliby WA, Randolph S, Koehler M, Hartmann LC, Slamon DJ. Expression of

p16 and retinoblastoma determines response to CDK4/6 inhibition in ovarian cancer. Clin Cancer Res 2011; 17(6): 1591–1602
8. Fassl A, Geng Y, Sicinski P. CDK4 and CDK6 kinases: from basic science to cancer therapy. Science 2022; 375(6577): eabc1495
9. Roberts JZ, Crawford N, Longley DB. The role of ubiquitination in apoptosis and necroptosis. Cell Death Differ 2022; 29(2): 272–284
10. Meng Y, Qiu L, Zhang S, Han J. The emerging roles of E3 ubiquitin ligases in ovarian cancer chemoresistance. Cancer Drug Resist 2021; 4(2): 365–381
11. Mir R, Tortosa A, Martinez-Soler F, Vidal A, Condom E, Pérez-Perarnau A, Ruiz-Larroya T, Gil J, Giménez-Bonafé P. Mdm2 antagonists induce apoptosis and synergize with cisplatin overcoming chemoresistance in TP53 wild-type ovarian cancer cells. Int J Cancer 2013; 132(7): 1525–1536
12. Allan LA, Skowyra A, Rogers KI, Zeller D, Clarke PR. Atypical APC/C-dependent degradation of Mcl-1 provides an apoptotic timer during mitotic arrest. EMBO J 2018; 37(17): e96831
13. Huang NJ, Zhang L, Tang W, Chen C, Yang CS, Kornbluth S. The Trim39 ubiquitin ligase inhibits APC/CCdh1-mediated degradation of the Bax activator MOAP-1. J Cell Biol 2012; 197(3): 361–367
14. Zhao G, Liu C, Wen X, Luan G, Xie L, Guo X. The translational values of TRIM family in pan-cancers: from functions and mechanisms to clinics. Pharmacol Ther 2021; 227: 107881
15. Ikeda K, Inoue S. TRIM proteins as RING finger E3 ubiquitin ligases. Adv Exp Med Biol 2012; 770: 27–37
16. Tian Y, Arai E, Makiuchi S, Tsuda N, Kuramoto J, Ohara K, Takahashi Y, Ito N, Ojima H, Hiraoka N, Gotoh M, Yoshida T, Kanai Y. Aberrant DNA methylation results in altered gene expression in non-alcoholic steatohepatitis-related hepatocellular carcinomas. J Cancer Res Clin Oncol 2020; 146(10): 2461–2477
17. Li Y, Gao J, Wang D, Liu Z, Zhang H. TRIM4 expression related to malignant progression and cisplatin resistance in osteosarcoma. Appl Biochem Biotechnol 2024; 196(1): 233–244
18. Driehuis E, Kretzschmar K, Clevers H. Establishment of patient-derived cancer organoids for drug-screening applications. Nat Protoc 2020; 15(10): 3380–3409
19. Beccaria M, Cabooter D. Current developments in LC-MS for pharmaceutical analysis. Analyst (Lond) 2020; 145(4): 1129–1157
20. Detre S, Saclani Jotti G, Dowsett MA. A "quickscore" method for immunohistochemical semiquantitation: validation for oestrogen receptor in breast carcinomas. J Clin Pathol 1995; 48(9): 876–878
21. Li RZ, Hou J, Wei Y, Luo X, Ye Y, Zhang Y. hnRNPDL extensively regulates transcription and alternative splicing. Gene 2019; 687: 125–134
22. Huang Y, Li S, Jia Z, Li S, He W, Zhou C, Zhang R, Xu R, Sun B, Ali DW, Michalak M, Chen XZ, Tang J. TRIM4 interacts with TRPM8 and regulates its channel function through K423-mediated ubiquitination. J Cell Physiol 2021; 236(4): 2934–2949
23. Freeman-Cook K, Hoffman RL, Miller N, Almaden J, Chionis J, Zhang Q, Eisele K, Liu C, Zhang C, Huser N, Nguyen L, Costa-Jones C, Niessen S, Carelli J, Lapek J, Weinrich SL, Wei P, McMillan E, Wilson E, Wang TS, McTigue M, Ferre RA, He YA, Ninkovic S, Behenna D, Tran KT, Sutton S, Nagata A, Ornelas MA, Kephart SE, Zehnder LR, Murray B, Xu M, Solowiej JE, Visswanathan R, Boras B, Looper D, Lee N, Bienkowska JR, Zhu Z, Kan Z, Ding Y, Mu XJ, Oderup C, Salek-Ardakani S, White MA, VanArsdale T, Dann SG. Expanding control of the tumor cell cycle with a CDK2/4/6 inhibitor. Cancer Cell 2021; 39(10): 1404–1421.e11
24. Braal CL, Jongbloed EM, Wilting SM, Mathijssen RHJ, Koolen SLW, Jager A. Inhibiting CDK4/6 in breast cancer with palbociclib, ribociclib, and abemaciclib: similarities and differences. Drugs 2021; 81(3): 317–331
25. Colon-Otero G, Zanfagnin V, Hou X, Foster NR, Asmus EJ, Wahner Hendrickson A, Jatoi A, Block MS, Langstraat CL, Glaser GE, Dinh TA, Robertson MW, Camoriano JK, Butler KA, Copland JA, Weroha SJ. Phase II trial of ribociclib and letrozole in patients with relapsed oestrogen receptor-positive ovarian or endometrial cancers. ESMO Open 2020; 5(5): e000926
26. Gu J, Chen J, Xiang S, Zhou X, Li J. Intricate confrontation: research progress and application potential of TRIM family proteins in tumor immune escape. J Adv Res 2023; 54: 147–179
27. Huang N, Sun X, Li P, Liu X, Zhang X, Chen Q, Xin H. TRIM family contribute to tumorigenesis, cancer development, and drug resistance. Exp Hematol Oncol 2022; 11(1): 75
28. Ma H, Qi G, Han F, Peng J, Yuan C, Kong B. PBK drives PARP inhibitor resistance through the TRIM37/NFκB axis in ovarian cancer. Exp Mol Med 2022; 54(7): 999–1010
29. Okamoto M, Kouwaki T, Fukushima Y, Oshiumi H. Regulation of RIG-I activation by K63-linked polyubiquitination. Front Immunol 2018; 8: 1942
30. Yan J, Li Q, Mao AP, Hu MM, Shu HB. TRIM4 modulates type I interferon induction and cellular antiviral response by targeting RIG-I for K63-linked ubiquitination. J Mol Cell Biol 2014; 6(2): 154–163
31. Marín I. Origin and diversification of TRIM ubiquitin ligases. PLoS One 2012; 7(11): e50030
32. Meroni G, Diez-Roux G. TRIM/RBCC, a novel class of 'single protein RING finger' E3 ubiquitin ligases. BioEssays 2005; 27(11): 1147–1157
33. Lorick KL, Jensen JP, Fang S, Ong AM, Hatakeyama S, Weissman AM. RING fingers mediate ubiquitin-conjugating enzyme (E2)-dependent ubiquitination. Proc Natl Acad Sci USA 1999; 96(20): 11364–11369
34. Batlle C, Yang P, Coughlin M, Messing J, Pesarrodona M, Szulc E, Salvatella X, Kim HJ, Taylor JP, Ventura S. hnRNPDL phase separation is regulated by alternative splicing and disease-causing mutations accelerate its aggregation. Cell Rep 2020; 30(4): 1117–1128.e5
35. Tsuchiya N, Kamei D, Takano A, Matsui T, Yamada M. Cloning and characterization of a cDNA encoding a novel heterogeneous nuclear ribonucleoprotein-like protein and its expression in myeloid leukemia cells. J Biochem 1998; 123(3): 499–507
36. Kamei D, Yamada M. Interactions of heterogeneous nuclear ribonucleoprotein D-like protein JKTBP and its domains with high-affinity binding sites. Gene 2002; 298(1): 49–57
37. Garcia-Pardo J, Bartolome-Nafria A, Chaves-Sanjuan A, Gil-Garcia M, Visentin C, Bolognesi M, Ricagno S, Ventura S. Cryo-EM structure of hnRNPDL-2 fibrils, a functional amyloid associated with limb-girdle muscular dystrophy D3. Nat Commun 2023; 14(1): 239
38. Lu HM, Li S, Black MH, Lee S, Hoiness R, Wu S, Mu W, Huether R, Chen J, Sridhar S, Tian Y, McFarland R, Dolinsky J, Tippin Davis B, Mexal S, Dunlop C, Elliott A. Association of breast and ovarian cancers with predisposition genes identified by large-scale sequencing. JAMA Oncol 2019; 5(1): 51–57
39. Wang Z, Gao J, Zhou J, Liu H, Xu C. Olaparib induced senescence under P16 or P53 dependent manner in ovarian cancer. J Gynecol Oncol 2019; 30(2): e26